國立臺灣大學醫學院病理學研究所

碩士論文

Graduate Institute of Pathology

College of Medicine

National Taiwan University

Master Thesis

微小乳突狀大腸直腸癌的臨床病理及分子特徵

The clinicopathological and molecular features of micropapillary colorectal carcinoma

林延儀

Yen-Yi Lin

指導教授：蔡佳惠 助理教授

Advisor: Jia-Huei Tsai, M.D. Ph.D.

中華民國 一百一十二 年 六 月

Jun, 2023

doi:10.6342/NTU202301505

國立臺灣大學碩士學位論文
口試委員會審定書

MASTER'S THESIS ACCEPTANCE CERTIFICATE
NATIONAL TAIWAN UNIVERSITY

中文題目:

微小乳突狀大腸直腸癌的臨床病理及分子特徵

英文題目:

The clinicopathological and molecular features of micropapillary colorectal carcinoma

本論文係林延儀君(學號: R10444006)在國立臺灣大學病理學研究所完成之碩士學位論文，於民國 112 年 6 月 27 日承下列考試委員審查通過及口試及格，特此證明

口試委員 Oral examination committee: _____ (簽名)

(指導教授 Advisor)

_____ _____

_____ _____

_____ _____

系主任/所長 Director: _____ (簽名)

摘要

微小乳突狀大腸直腸癌被認為是一種預後不良的大腸直腸癌，與淋巴血管和周圍神經侵犯呈現高度相關。微小乳突狀大腸直腸癌的定義為在所有腫瘤部位中至少有 5%的微小乳突狀結構。組織學上，它由缺乏纖維血管性核心的微小乳突狀細胞團塊所構成且被緻密的纖維基質和空腔包圍。微小乳突狀細胞瘤因其細胞極性反轉呈現特殊的 “inside-out”結構。

在這項研究中，我們調查了 2008 年至 2012 年在國立台灣大學醫院切除的 2148 例大腸直腸癌樣本並診斷出 49 例微小乳突狀大腸直腸癌。並分析其臨床和病理特徵來進行研究。臨床特徵顯示微小乳突狀大腸直腸癌主要出現於男性並偏好於大腸左側。預後因子的分析中顯示微小乳突狀大腸直腸癌的分化較差且易出現高比例的腫瘤出芽和分化不良腫瘤團塊。腫瘤出芽和分化不良腫瘤團塊是目前新興的大腸直腸癌預後指標而且其與微小乳突狀大腸直腸癌的形態學相似。有趣的是，在多變量分析中，腫瘤出芽的比例比起分化不良腫瘤團塊的比例或診斷是否為微小乳突狀大腸直腸癌在預測病人預後上扮演著相對重要的角色。因此應優先考慮腫瘤出芽作為大腸直腸癌患者的預後指標。

之後我們利用標的次世代基因定序研究微小乳突狀大腸直腸癌提的分子特徵。經過驗證後我們發現 *TP53*（10/12，92%）和 *APC*（8/12，75%）突變率非常高，而 *KRAS*（2/12，17%）突變率則較一般大腸直腸癌低。因此，我們進一步用免疫組織化學染色和桑格測序法去延伸次世代基因定序的結果。在我們研究群體中，微小乳突狀大腸直腸癌具有高比例 p53 的表現異常（47/49, 96%）、*RAS* / *RAF* 熱點突變率低 （*RAS*: 10/49, 20%; *RAF*: 2/49, 4%）、及完全保留錯配修復蛋白染色（49/49, 100%）。綜合以上研究，微小乳突狀大腸直腸癌有著獨特的臨床病理及分子特色，不同於一般大腸直腸癌，可視為是獨特的型態學分類。

doi:10.6342/NTU202301505

關鍵詞：微小乳突狀癌、大腸直腸癌、腫瘤出芽、分化不良腫瘤團塊、 *TP53*、*RAS/RAF*

doi:10.6342/NTU202301505

Abstract

Micropapillary colorectal carcinoma (MicCRC) is a subtype of colorectal cancer (CRC), characterized by poor prognosis, high lymphovascular, and perineural invasion. MicCRC is defined as having at least 5% of micropapillary structure in the tumor. Histologically, it is characterized by small papillary clusters of neoplastic cells that lack fibrovascular cores and are surrounded by dense fibrous stroma and lacunar spaces. Micropapillary carcinoma exhibits an "inside-out" pattern which shows reverse cell polarity. In this study, we investigated the clinical and pathological characteristics of 49 MicCRCs identified from 2128 resected CRC specimens at National Taiwan University Hospital from 2008 to 2012. Our results showed that MicCRC predominantly affects males and originates in the left side of the large intestine. It is associated with high-grade differentiation, tumor budding, and poorly differentiated clusters (PDCs). Tumor budding and PDCs share similar morphology with MicCRC and are new prognostic indicators in CRC, being associated with high tumor grade and advanced TNM stages. In multivariate analysis, tumor budding was found to play a critical role as a prognostic indicator in our cohort, rather than PDCs or diagnosis of MicCRC. Therefore, tumor budding should be given high priority as a prognostic indicator in CRC patients.

Our current understanding of the molecular pathways involved in MicCRC is still relatively preliminary. We submitted 12 MicCRCs to targeted next-generation sequencing

doi:10.6342/NTU202301505

to investigate the molecular features of MicCRC. The results demonstrated high mutation rates in *TP53* (10/12 ,92%) and *APC* (8/12, 75%), low mutation rate in *KRAS* (2/12, 17%). Therefore, we utilized immunohistochemical and sanger sequencing to validate the results of NGS. We recognized that MicCRC exhibited high rate of aberrant p53 expression (47/49, 96%), preserved MMR expression (49/49, 100%), and low rate of *RAS*/*RAF* hotspot mutations (*RAS*: 10/49, 20%; *BRAF*: 2/49, 4%) in our cohort. These findings suggest that the molecular pathways involved in MicCRC differ from those in conventional CRC.

Key words: Micropapillary carcinoma, colorectal carcinoma, tumor budding, poorly differentiated clusters, *TP53*, *RAS/RAF*

doi:10.6342/NTU202301505

Contents

doi:10.6342/NTU202301505

doi:10.6342/NTU202301505

1. Introduction

Colorectal cancer (CRC) has been reported as the third most-common cancer in the world.[1] CRCs display different pathogenesis and molecular functions, indicating variable incidence, phenotype, and prognosis.[2] Although part of the pathophysiology of CRC has been completely studied, the molecular mechanism of certain phenotypes remains unclear.

The micropapillary pattern is a well-established histological subtype associated with poor prognosis in CRCs, representing 9-19% of all CRCs.[2] Initially identified in breast cancer, this pattern has subsequently been observed in cancers from other organs, including the urinary bladder, lung, ovary, and salivary gland.[3] For a diagnosis of micropapillary colorectal carcinoma (MicCRC), the micropapillary pattern must account for at least 5% of the total tumor area. Histologically, micropapillary carcinoma is characterized by small papillary clusters of neoplastic cells that lack fibrovascular cores and are surrounded by dense fibrous stroma and lacunar spaces.[4-6] These clusters are separated by delicate strands of fibrous tissue, creating a sponge-like structure.[3-5] The arrangement of micropapillary clusters is regular and the neoplastic cells exhibit eosinophilic cytoplasm and pleomorphic nuclei when stained with hematoxylin and eosin stain. Furthermore, the clusters display an "inside-out" pattern in which the cell polarity of the micropapillary nests displays a reverse configuration, with their apical surfaces facing the periphery rather than the center.[3, 6, 7] This reverse polarity is in contrast to the

doi:10.6342/NTU202301505

histology of conventional CRC patterns where the apical membrane lines the inside of the lumen formed on the opposite side of the basal membrane and extracellular matrix.[8]

MicCRC has been identified as an aggressive subtype of CRCs with a poor prognosis.[9-11] While the TNM classification system remains the gold standard for predicting the prognosis of CRCs patients, there is still considerable variability in outcomes among patients with the same TNM stage. As such, there is a need of additional biomarkers to improve prognostic accuracy. Commonly used indicators include differentiation, lymphovascular invasion, perineural invasion, and molecular factors[12]. Previous studies have reported that MicCRC exhibits a higher proportion of vascular invasion compared to conventional CRC,[11, 13, 14] and that the presence of micropapillary features has independent prognostic significance in TNM stages 1 and 2.[11] Recent researches have identified several new indicators to improve the prognosis of CRC.[15] Tumor budding is one of new prognostic indicators in CRC, being associated with high tumor grade, advanced TNM stage, lymphovascular invasion, and distant metastases.[16, 17] Tumor budding is defined as the presence of single cells or clusters of up to four cells under a 0.785 mm^2 microscopic field.[18] In contrast, clusters of five or more cells are identified as poorly differentiated clusters (PDCs). These clusters are more likely to be observed in the invasive front of CRC. PDCs were first described by Ueno in 2012 as a new criterion for evaluating the prognosis of CRC and are recognized as a poor prognostic factor.[19] Recent

doi:10.6342/NTU202301505

research suggests that MicCRC and PDC may be a part of spectrum due to their histological similarities, including reversed MUC1 expression of tumor cell.[14, 20] While PDCs share morphological similarities with MicCRC, there are notable differences between these phenotypes. Histological features such as cleft-like spaces and glandular differentiation, are seen in MicCRC clusters but not in PDCs.[9, 21] MicCRC usually appears as a distinct group arising from conventional CRC while PDCs are more randomly distributed. The percentage of MicCRC can vary from 5% to 100% while PDCs account for a smaller proportion of CRC. Until now, it is not known whether tumor budding, PDCs, and MicCRC are independent predictors of the prognosis of CRC. Further research is required to determine the impact of tumor budding, PDCs and micropapillary histology on the survival of CRC.

Molecular pathways play a significant role in the prognosis and occurrence of CRCs.[22] A deeper understanding of the molecular mechanisms underlying the formation of MicCRC can aid in predicting its prognosis. Previous studies have shown that the aberrant activation of the RhoA/ROCK pathway plays a critical role in the inability to switch cell polarity both in vivo and in vitro, potentially leading to the "inside-out" pattern observed in MicCRC.[8] Additionally, clinical research has indicated that microsatellite instability is uncommon in MicCRC patients. Gene mutations in MicCRCs frequently occur in *KRAS* and *TP53*. A 2022 study on invasive micropapillary carcinoma of the breast found that

doi:10.6342/NTU202301505

TP53 mutations were predominant in their whole exome sequencing results.[23] Previous research on micropapillary carcinoma of the urinary bladder has investigated its pathways through whole-genome mRNA expression data. The findings suggest that genes anomalies associated with the p53 and RhoA pathways are in micropapillary carcinoma cells.[24] Furthermore, several studies have identified *TP53* mutations using IHC methods in MicCRC patients, with altered p53 expression being more common in MicCRC.[25] *KRAS* mutations may also serve as a prognostic factor for CRC, as they are associated with poorer prognosis and resistance to certain treatments. Previous results have indicated that the frequency of *KRAS* mutations in MicCRC is similar to that of CRC without the micropapillary phenotype.[25, 26] Until now, our current understanding of the molecular pathways involved in MicCRC remains elusive. In our current study, we utilized targeted next-generation sequencing to gene mutations of MicCRC. Our goal is to identify unique genetic mutations in MicCRC that could contribute to its phenotype and prognostic outcome.

doi:10.6342/NTU202301505

2. Material and Methods

2.1 Tissue specimens.

We reviewed 2128 CRCs from 2008 to 2012 and identified 49 MicCRCs. We specifically selected 12 MicCRCs that had sufficient micropapillary structures to ensure enough tissue for targeted next-generation sequencing molecular analysis. Two hundred conventional CRCs were randomly selected as a control cohort. All the patients underwent complete staging surgery. Hematoxylin & Eosin stained slides were retrieved from the archives of the Department of Pathology, National Taiwan University Hospital. Our study was conducted in accordance with the regulations of the Ethics Committee, and the specimens were analyzed anonymously and in a blinded manner. We staged the tumors according to the 7th AJCC system,[27] and we considered tumors to be on the right side if they were located in the cecum, ascending colon, hepatic flexure or transverse colon, and on the left side if they were located in splenic flexure, descending colon, sigmoid colon, rectosigmoid colon, or rectum.

2.2 Morphologic review.

In this study, histologic sections of 4-μm thickness were prepared and stained with hematoxylin and eosin. These sections were examined to determine the percentage of micropapillary clusters, histologic grading, presence of lymphovascular invasion, perineural invasion, grading of tumor buddings, and PDC. Lymphovascular invasion

doi:10.6342/NTU202301505

was identified as the presence of cancer cells in lymphatic or blood vessels located adjacent to or within the tumor. Perineural invasion was described as the invasion of cancer cells into the nerves.

To assess tumor budding, the tumor histologic sections were scanned at low magnifications (40×) on Olympus BX53 microscope in one hotspot at the invasive front. The tumor buddings were assessed in a microscopic field of 0.785 mm^2, and the tumor bud count was normalized from a specimen area of 0.95 mm^2.[18] A 2-tier system was used to grade tumor buddings based on the number of tumor cell clusters present in the examined field. Tumor buddings with 10 or more cell clusters of ≤ 4 tumor cells in the examined field were classified as high-grade, while those with fewer than 10 cell clusters were classified as low-grade. PDCs were graded in the same way as tumor buddings in X20 objective lens but the clusters were aggregates of 5 or more cancer cells without glandular formation.[19]

2.3 Statistical analysis.

Data were analyzed using SPSS 26.0 software (IBM Corp., Armonk, NY, USA). Comparisons of categorical variables were performed using the Pearson x^2 method or Fisher exact test when appropriate. Statistical calculation was applied using Student's t test for continuous variables. The survival curves were generated using the Kaplan–Meier method, and the differences were calculated using the log-rank test. The Cox

doi:10.6342/NTU202301505

proportional hazards regression model was used to compare the differences in the survival rates in univariate and multivariate analyses. All statistical results were considered significant at $P < 0.05$.

2.4 DNA extraction and targeted next-generation sequencing.

For this study, targeted areas of tumor were marked on a representative H&E-stained section of each tumor. These marked areas from 10-μm paraffin sections were dissected using sterilized razors. Genomic DNA was extracted from those dissected area using a QIAamp DNA FFPE Tissue Kit (Qiagen, Santa Clarita, CA, USA) fallowing the manufacturer's protocol. The study used a custom-designed amplicon-based panel for targeted NGS that includes 275 genes known to be pathogenic in human cancers (Supplementary Table 1). For library preparation, the study used a total of 100ng gDNA per FFPE sample and generated sequencing libraries using QIAseq Comprehensive Cancer Panel (Qiagen, cat. #DHS-3501Z), following the manufacturer's recommendations. The initial steps for preparing genomic DNA samples involve fragmenting the DNA, repairing the ends, and adding an A-tail using a controlled multi-enzyme reaction. Then, the prepared DNA fragments were ligated with a sequencing platform-specific adapter containing UMIs and sample index at their 5' ends. Each original DNA molecule is assigned a unique sequence called a UMI. The adaptor-ligated DNA libraries are subject to several cycles of targeted PCR using one panel of loci -

doi:10.6342/NTU202301505

specific primers and one universal primer complementary to the adapter for target enrichment. The study used a universal PCR to amplify the library and add specific adapter sequences and additional sample index. The libraries were denatured and sequenced on Illumina HiSeq x-ten platform and 150bp paired-end reads were generated with an average depth is 2,000X coverage per sample by Genomics BioSci & Tech Co. Sequence alignment to a reference genome was performed using Burrows-Wheeler Aligner (BWA). Somatic mutations were detected using the smCounter workflow and all detected variants with a minimum coverage depth of 100 reads were filtered for known single nucleotide polymorphisms (SNPs) using the Exome Sequencing Project databases and annotated by searching the Variant Effect Predictor (https://asia.ensembl.org/info/docs/tools/vep/index.html).

2.5 Validation by Sanger sequencing method.

A subsequent search in the COSMIC catalogue was performed to identify driver mutations. We validated missense mutations with unknown significance in the COSMIC database. To determine the deleterious nature of the missense mutations, we used online programs such as SNPs&GO (http://snps.biofold.org/snps-and-go/snps-and-go.html), PolyPhen-2 (http://genetics.bwh.harvard.edu/pph2/), and COSMIC (https://cancer.sanger.ac.uk/cosmic). To confirm the results of the mutations detected by NGS, we validated some pathogenic mutations recorded in the COSMIC database, such

doi:10.6342/NTU202301505

as mutations in *KRAS, BRAF, NRAS,* and *TP53* genes. We amplified our samples using Touch-down PCR, followed by electrophoresis to check their base pairs. Primers we use for PCR are summary in supplementary table 2. Then, we entrusted our samples to Genomics Company (Taipei, Taiwan), where they underwent sanger sequencing using a 3730xl DNA Analyzer (ThermoFisher, Waltham, USA). Finally, we analyzed all the sanger sequencing data using Chromas 2.6.6 (Technelysium Pty Ltd, South Brisbane, Australia).

2.6 Immunohistochemical validation.

The tissue sections (4 μm) obtained from paraffin-embedded arrayed tissue were subjected to deparaffinization using the Ventana Discovery XT platform (Ventana/Roche, Mannheim, Germany). This was achieved by incubating the sections with EZ prep solution (Ventana/Roche, Mannheim, Germany) at 65°C for 15 minutes. The sections were then stained using the OptiView DAB IHC Detection Kit (Ventana/Roche, Mannheim, Germany) on the Ventana Discovery XT platform fallowing the manufacturer's protocol. The sections were subjected to antigen retrieval using Cell Conditioning Solution (CC1, Tris-EDTA based buffer pH 7.8, Ventana/Roche, Mannheim, Germany) at 95°C for a duration that depends on the primary antibody and the type of tissue. After blocking with inhibitor at 37°C for 4 minutes, the sections were incubated with primary antibodies against MSH6 (clone SP93, 1:1, Cell Marque - Sigma-Aldrich,

doi:10.6342/NTU202301505

Rocklin, USA), PMS2 (clone A16-4, 1:1, Ventana/Roche, Mannheim, Germany), and p53 (clone D07, 1:200, Cell Marque - Sigma-Aldrich, Rocklin, USA) for a duration that depends on the primary antibody. Following incubation, OptiView HRP Multimer was applied and incubated for 16 minutes. The slides were then incubated with DAB and H_2O_2 for 8 minutes and subsequently incubated with copper solution for 5 minutes. Finally, the sections were counterstained with hematoxylin for 8 minutes.

doi:10.6342/NTU202301505

3. Results

3.1 Morphology of MicCRC & prognosis factors

Micropapillary structures were found from 5% to 100% of the tumors in MicCRC. The percentage of MicCRC was 5% – 10% in 16/49 (33%), 10% – 50% in 12/49 (24%), and >50% in 29/49 (59%). Figure 1a-f showed the typical features of these structures, which are tightly packed invasive clusters within lacunar spaces with retraction-like spaces from the stroma (Figure 1a 40x, 1b 200x). Micropapillary clusters do not have fibrovascular cores. The tumor cells have a reversed polarity, with their apical surfaces facing the stroma and an "inside-out" pattern. Tumor cells often displayed dense cytoplasmic eosinophilic and nuclear pleomorphism. Other prognostic factors were also investigated such as tumor buddings (Figure 1c), high-grade PDCs (Figure 1d), lymphovascular invasion (Figure 1e), and perineural invasion (Figure 1f).

3.2 Clinical characteristic of MicCRC

The clinical characteristic of MicCRC were summarized in Table 1. In study cohort, men were predominant, accounted for 67 percent of all cases (n=33/49, 67%). The average age of MicCRC patients was 66 years old (range 34-86). Tumors originated in the left side of the large intestine accounted for a substantial fraction of MicCRC patients (n=39/49,80%). Subsequently, we interpreted the prognostic factors of H&E slides. Tumor differentiation was classified as high-grade in 53% of MicCRC (n=26/49, 53%) and low-grade in 47 %

doi:10.6342/NTU202301505

(n=23/49, 47%). High-grade PDC was observed in all MicCRCs (n=49/49, 100%). The frequency of high-grade tumor budding in the study group was approximately 67 % (n=33/49, 67%). Lymphovascular and perineural invasion was shown in MicCRC at a prevalence of 65% (n=32/49, 65%) and 39% (n=19/49, 39%). The distribution of TNM anatomical stage in our study cohort was stage I in 14% (n=7/49), stage II in 39% (n=12/49), stage III in 41% (n=20/49), and stage IV in 20% (n=10/49). We compared the clinical feature of our study cohort and investigated the difference between MicCRC (n=49) and control cohort of conventional CRC (n = 200). MicCRCs were more common in male (Figure 2a), in contrast to conventional CRCs (P = 0.018). There were no differences in the ages of two groups, both were approximately 65 years old (Figure 2b, P = 0.453). Nearly 80 percent of MicCRCs had tumor patients at left side of the large intestine (Figure 2c, P = 0.024) higher than the control group (n=125/200, 63%). The prognostic factors of the two groups were then compared. Tumor differentiation (Figure 2d, P < 0.001), PDC (Figure 2e, P < 0.001), and tumor budding (Figure 2f, P < 0.001) displayed high degree of distinction between MicCRCs and CRCs. High-grade tumor differentiation (n=31/200,16%), high-grade PDC (n=71/200, 36%) and high-grade tumor budding (n=67/200,34%) were less commonly identified in the control CRC group. The ratio of lymphovascular and perineural invasion did not show significant difference between MicCRC and control group. Lymphovascular invasion was seen in 69% of all

doi:10.6342/NTU202301505

control cases (n=137/200, 69%), similar to MicCRC groups (Figure 2g, P = 0.668). No differences were observed in perineural invasion (Figure 2h, P = 0.33). The distribution of TNM anatomical stage also showed no differences between MicCRC and control group (Figure 2i, P = 0.632). The control CRC cases were classified as stage I in 17% (n=34/200), stage II in 29% (n=57/200), stage III in 31% (n=62/200), stage IV in 24% (n=47/200). The comparison was all summarized in Table 2.

3.3 Survival rates under different factors

In order to understand the influence of each factor in our study on the prognosis, we then tracked and analyzed their survival rate. We divided the study cohort into groups with different prognostic factors, we then estimated their survival curves using the Kaplan-Meier (K-M) method (Figure 3a- i). Gender had little effects on CRC prognosis (Figure 3a, log-rank, P = 0.263). Among the sides of the colon where CRCs developed, the left side had a tendency of better survival than the right side (Figure 3b, log-rank, P = 0.064). CRCs with high-grade differentiation exhibited worse survival than those with low-grade differentiation in our cohort (Figure 3c, log-rank, P < 0.001). Survival rate analysis showed no significant difference between MicCRC and CRC groups (Figure 3d, log-rank, P = 0.626). Both CRCs with high-grade tumor budding and CRCs with high-grade PDC showed worse survival compared with CRCs with low-grade tumor budding (Figure 3e, log-rank, P < 0.001) and low-grade PDC (Figure 3f, log-rank, P < 0.001). Lymphovascular

doi:10.6342/NTU202301505

invasion was an aggressive factor in assessing the prognosis of CRC (Figure 3g, log-rank, $P < 0.001$). K-M curves from our cohort showed that survival of CRC patients with perineural invasion was lower than that of patients without perineural invasion (Figure 3h, log-rank, $P < 0.001$). TNM anatomical stage was a strong prognostic factor in CRCs (Figure 3i, log-rank, $P < 0.001$). These data suggested that differentiation, tumor budding, lymphovascular invasion, perineural invasion, and TNM anatomical stage but not diagnosis of MicCRC were striking prognostic factors to predict prognosis.

3.4 Multivariate analysis

We collected data including their age, sex, tumor location, diagnosis of MicCRC, tumor differentiation, tumor budding, PDC, lymphovascular invasion, perineural invasion and TNM stages and submitted the factors into Cox regression analysis to evaluate the multivariate survival analysis (Table 3).

In multivariate survival analysis, the statistics of sex, lymphovascular invasion, and PDC were not significant. The hazard ratio for sex status was 1.003 (95% confidence intervals: 0.661-1.524, $P = 0.987$), for lymphovascular invasion was 0.906 (95% confidence intervals: 0.482-1.703, $P = 0.759$), and PDC was 0.718 (95% confidence intervals: 0.419-1.231, $P=0.228$). In both univariate and multivariate analyses, age, tumor differentiation, tumor budding, and perineural invasion are strong prognostic factors for

doi:10.6342/NTU202301505

survival in patients with CRC. In multivariate analysis, the hazard ratios for these factors were 1.031 (95% confidence intervals:1.013-1.050, P = 0.001), 2.420 (95% confidence intervals: 1.451-4.035, P = 0.001), 3.280 (95% confidence intervals: 1.924-5.591, P < 0.001), and 1.999 (95% confidence intervals: 1.224-3.266, P = 0.006), respectively. The Hazard ratios for cancer stages I, II, and III (compared to stage IV) were 0.085 (95% confidence intervals: 0.028-0.261), 0.120 (95% confidence intervals: 0.062-0.232), and 0.218 (95% confidence intervals: 0.133-0.356), respectively (P < 0.001). MicCRCs histology was a significant prognostic factor in multivariate analysis. The hazard ratio for the diagnosis of MicCRCs was 0.479 (95% confidence intervals: 0.258-0.888, P = 0.02), indicating that patients with MicCRCs have a 52.1% lower risk of death than patients with CRCs.

3.5 Targeted next-generation sequencing of MicCRC

In order to understand the molecular characteristic of MicCRC, we submitted 12 samples to targeted next-generation sequencing using QIAseq Comprehensive Cancer Panel. The NGS results displayed gene annotation variants as shown in Figure 4. To determine whether the gene alterations were pathological, we validated the data using online databases, Sanger sequencing, and IHC methods. Our results after validation, summarized in Figure 5, revealed that *TP53* (11/12,92%) and *APC* (9/12,75%) were the two most-commonly mutated genes in MicCRCs. Our study found mutations in the

doi:10.6342/NTU202301505

MUYTH gene (2/12, 17%) in two samples of MicCRC. The mutation spot of *TP53* and *APC* were displayed in Figure 6a-b. Other mutated genes of our results such like *FBXW7* (3/12, 25%), *AMER1* (1/12, 8%), were also correlated with Wnt pathway.[28] Our results identified that *SOX9* (1/12, 8%), a gene encoding a transcription factor, had a stop gained mutation, indicating a loss of function. We also observed mutations in *TGFBR2* (2/12, 17%) and *SMAD2* (1/12, 8%), which encode proteins that participate in the TGF-β pathway. Our samples exhibited mutations in *TGFBR2* and *SMAD2*, indicating that the TGF-β pathway may also play a role in the development of MicCRC. Our findings showed that mutations in the genes *ARID1B* (2/12, 17%) and *PBRM1*(1/12, 8%) in samples of MicCRC. Our study also found mutations in *TSC2* (2/12, 17%). Supplementary Table 3 contains a detailed description of the genes that were found to have mutations in our study. Supplementary Table 4 provides information on genes that showed of uncertain significance.

3.6 Molecular features of MicCRC

Our NGS results showed that *TP53* is one of the prevalent mutated genes in MicCRC cells. A previous study had also found that *TP53* was the most frequently mutated gene in a micropapillary breast cancer.[23] Based on these findings, we performed immunohistochemistry (IHC) staining using anti-P53 to determine the aberrant rate in our cohort (Figure 7a-c). The aberrant expression of p53 was classified as overexpressed

doi:10.6342/NTU202301505

(Figure 7a) or lost (Figure 7b), indicating a mutated type. The wild type showed weak expression (Figure 7c).[29] We found that 96% of MicCRC patients (47 out of 49) had aberrant expression of p53, while only 66% of control CRC patients (33 out of 50) had aberrant expression of p53 (Figure 7d, P<0.001). The aberrant expression of p53 was found to be significantly higher in MicCRC patients, indicating a strong association between p53 abnormality and MicCRC (Table 4).

In our NGS results, genes associated with mismatch repair proteins (MMRs) were not mutated. Therefore, we performed MMR immunohistochemistry (Figure 7e-f) on our MicCRC samples to investigate mismatch repair protein integrity. The data showed that neither PMS2 (49/49, Figure 7e) nor MSH6 (49/49, Figure 7f) showed loss of expression in all MicCRC samples. These data suggested that MicCRC were mostly MMR proficient.

RAS and *RAF* genes are well-known tumor oncogenes in CRC. These mutations are associated with a poorer prognosis and resistance to certain types of treatments. Our NGS results (Figure 5.) revealed that few samples exhibited few mutations in *KRAS* mutations (2/12, 17%) in MicCRCs with one concurrent mutation in *NRAS* (1/12, 8%). To investigate this further, we performed Sanger sequencing to detect the hotspots of *KRAS, NRAS*, and *BRAF* in our MicCRC samples. Our findings showed that 20% of MicCRC patients (n=10/49) had *KRAS* mutations, including 3 cases of c.35G >A, p. Gly12Asp, 2 case of c. 38G >A, p. Gly13Asp and 4 cases of c.35G >T, p. Gly12Val. One case had both

doi:10.6342/NTU202301505

KRAS (c.35G >A, p. Gly12Asp) and *NRAS* (c.35G >T, p. Gly12Val) mutation. In contrast, only 2% of MicCRC had *BRAF* (n=2/49) mutations including 1 case of c.1799T >A, p. Val600Glu, and 1 case of c.1780G>A, p. Asp594Asn. All of the sanger sequencing data were summarized in Table 5.

doi:10.6342/NTU202301505

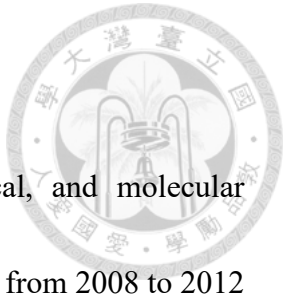

4. Discussion

Our research focused on investigating the clinical, pathological, and molecular characteristics of MicCRC. We screened 2128 cases of resected CRC from 2008 to 2012 from National Taiwan University Hospital and identified only 49 MicCRCs (2.3%). The prevalence was lower than the incidence reported in previous studies, which observed MicCRCs in 9-19% of CRCs.[2] The discrepancy may result from criteria we used in this study to diagnose MicCRC and our tendency to separate PDC from MicCRC.

Clinically, MicCRCs predominantly affects males and more often originate in the left-side of the large intestine, as compared to control CRCs. Evaluating the side of the colon can be used to predict the molecular function of CRC, as left-side CRCs are predominantly associated with chromosomal instability pathway, and right-side CRCs that are more associated with microsatellite instability-high tumors.[30] MicCRC patients in our cohort were all MMR proficient, which corresponds to only 20% of the right-side tumor location.

MicCRC is considered a poor prognosis phenotype in previous research.[4, 9, 11] Our data demonstrated that MicCRCs were more commonly associated with poor prognostic characteristics, such as high-grade differentiation, high-grade tumor budding, and high-grade PDCs than control CRCs. High-grade differentiation and tumor budding were associated with poor overall survival. Previous researches have also showed that tumor

doi:10.6342/NTU202301505

budding, [31] PDCs, [32] and high-grade tumor differentiation [33] are indicators of poor prognosis. However, our results demonstrated that the micropapillary phenotype shared similar survival rate with the control group in the Kaplan-Meier analysis. In multivariate survival analysis, the control CRCs even showed higher hazard ratio than MicCRC. High-grade tumor budding remained a dismal predictor in multivariate survival analysis. Because MicCRC displays morphologic similarity with tumor budding and PDCs,[14, 17, 21] it is plausible that CRC with tumor budding or PDC might be mis-diagnosed as MicCRC in previous studies. Because tumor budding and PDCs were both poor prognostic factors, it is not surprised that MicCRC would be reported as an aggressive tumor if they were actually CRC with tumor budding or PDCs.[19] Histologic findings of high-grade PDCs include the presence of over 10 cancer clusters in the invasive front composed of at least five tumor cells in a defined field,[19, 32, 34] whereas tumor budding clusters are composed of fewer than five tumor cells.[16] PDCs are clusters of cancer cells without glandular differentiation and with varying sizes, surrounded by desmoplastic stroma. In contrast, classic micropapillary clusters may contain glandular structures and have noticeable cystic spaces-like clefts.[21] Upon screening the CRC slides, we observed that clusters of MicCRC often appeared as distinct groups of micropapillary histology, in contrast to PDC clusters which were more likely randomly located at the tumor invasive front. Therefore, we diagnosed MicCRC not only in tumor with at least of 5% micropapillary pattern but

doi:10.6342/NTU202301505

also the classic micropapillary structures occurring as distinct tumor groups. In contrast, CRC with PDC often displayed random distribution of PDCs without distinct aggregation. In addition, MicCRC may account for more than 50% of all CRC tumor part while CRC with PDC usually showed a minor proportion of PDC component. Furthermore, in a study by Mineui Hong et al.,[21] it was observed that PDCs lacked MUC1 expression in the tumor center, whereas in MicCRC, MUC1 was expressed in the all of the micropapillary clusters.[7] Based on these findings, we propose that the micropapillary pattern is different from both tumor buddings and PDCs. In particular, tumor budding should be given priority as a prognostic indicator in CRC patients.

KRAS mutations are a crucial molecular feature in investigating the prognosis of CRC. Previous studies have reported high *KRAS* mutation rates in MicCRC patients. For instance, Gonzalez RS et al. reported a 45% (27/60) mutation rate in their MicCRC cohort,[4] while Raul S. Gonzalez reported a 35% (11/31) mutation rate in their study.[26] However, our research found a significantly low *KRAS* mutation rate with only 20% in MicCRC. This discrepancy may be due to differences in the study cohorts. Interestingly, PDC has been reported to exhibit a positive correlation between its grade and *KRAS* mutation rate.[35] It is possible that high *KRAS* mutations in MicCRC reported in previous studies may be partially contributed from *KRAS*-mutated CRC with PDC. These findings suggest that the difference in *KRAS* mutation rates between MicCRC and PDC could be

doi:10.6342/NTU202301505

attributed to variations in the study cohorts and the grade of PDC. This may also explain the high occurrence rate of MicCRC in CRC in previous studies, which may include some CRC with PDC but not actually MicCRC. Our study demonstrated different clinicopathologic features and molecular features between MicCRC and CRC with PDC, we considered that MicCRC and PDC should be considered as distinct phenotypes.

Next-generation sequencing of our study cohorts indicated that *TP53* mutations prevail in MicCRC. High *TP53* mutation was also observed in micropapillary breast cancer.[23] Additionally, an early study of MicCRC also found a higher proportion of *TP53* alterations by using IHC methods.[4] With aids of P53 IHC staining, our study identified that most but not all MicCRCs harbored aberrant p53 expression. This finding was consistent with previous researches. [4, 23] Mutations of *TP53* were closely associated with tumorigenesis, as it encodes the protein p53, which is a crucial transcription factor. The primary function of p53 is to regulate responses that are primarily responsible for controlling the cell cycle.[36] Recent research has revealed that the Rho/Rock signaling pathway plays a critical role in reversing the cell polarity of MicCRC cells.[8] Aberrant activation of RhoA promoted polarity switching of CRC glands, resulting in an "inside-out" morphology pattern and micropapillary histology. On the other hand, tumor cells with *TP53* mutations have been shown to alter cell polarity and morphological features, resulting in increased migration.[25, 37-39] Loss of p53 cooperates with activated Ras in

doi:10.6342/NTU202301505

colonic epithelial cells to synergistically induce RhoA activity, resulting in increased cell motility.[39] Gain of function of p53 mutants can also affect integrin signaling by increasing integrin signaling and upregulating RhoA protein.[38] Based on these studies, we suggest that *TP53* mutations are closely associated with aberrant RhoA activation and play a role in reversing cell polarity with formation of micropapillary histology. This could be the a reason that *TP53* mutations are highly frequent in MicCRCs.

Our study also found mutations in the *MUTYH* gene (2/12, 17%) in our samples of MicCRC. *MUTYH* is a downstream gene that mediates p53 tumor suppression and induces cell apoptosis under oxidative stress.[40] This suggests that one of the pathways related to p53 may also be involved in the development of MicCRC. *APC* was another common mutation in MicCRC. *APC* is known as a tumor suppressor gene, which regulates cell proliferation and differentiation by inhibiting the Wnt signaling pathway. Mutation of *APC* is the main driver of Wnt signaling in CRC. Other mutated genes of our results such like *FBXW7* (3/12, 25%), *AMER1* (1/12, 8%), are also correlated with Wnt pathway.[28] *FBXW7* encodes an E3 ubiquitin ligase that is involved in the ubiquitination and degradation of several key components of the Wnt pathway. *AMER1* acts as a negative regulator of the Wnt pathway by binding to the β-catenin destruction complex, which helps to regulate the levels of β-catenin in the cell. Our results have shown that *SOX9* (1/12, 8%), a gene encoding a transcription factor, has a stop gained mutation,

doi:10.6342/NTU202301505

indicating a loss of function. Previous research has demonstrated that *SOX9* can act as an inhibitor, down-regulating the Wnt pathway in colorectal cancer.[41] Our data suggested that mutations in the Wnt pathway also plays a significant role in the formation of MicCRC. We also observed mutations in *TGFBR2* (2/12, 17%) and *SMAD2* (1/12, 8%), which encode proteins that participate in the TGF-β pathway. In this pathway, TGFBR2 acts as a receptor that activates downstream proteins like SMAD2, regulating the transcription of target genes. This pathway can either promote cell cycle arrest and apoptosis or induce tumor metastasis, depending on the stage of the tumor cell.[42] MicCRC also exhibited mutations in *TGFBR2* and *SMAD2*, indicating that the TGF-β pathway may also play a role in the development of MicCRC. Meanwhile, mutations in *ARID1B* (2/12, 17%) and *PBRM1*(1/12, 8%) were present in a few samples of MicCRC. These genes encode proteins that belong to different subunits of the SWI/SNF complex, which plays a vital role in chromatin remodeling and transcriptional regulation. In recent years, SWI/SNF complex has been found to be associated with tumor suppression, inactivating mutations in these genes have been detected in various types of tumors.[43] Therefore, our results suggest that SWI/SNF complex may also be involved in the development of MicCRC. Previous research has demonstrated that TSC2 plays a crucial role in goblet cell differentiation by inhibiting the mTOR pathway in intestinal cell lines.[44] Our study has found mutations in *TSC2* (2/12, 17%). Overall, based on the above findings, this study

doi:10.6342/NTU202301505

identified *TP53* aberrations and Wnt pathway activation were the characteristic molecular features of MicCRC. A low RAS/RAF mutation rate and MMR proficiency was also observed in MicCRC. The distinct molecular phenotypes distinguish MicCRC from conventional CRC.

Our study has some limitations regarding the molecular characteristics of MicCRC. Firstly, the small sample size of only 12 submitted for NGS panel analysis may overlook certain mutations specific to MicCRCs. Secondly, the mutation gene panel focuses on genes commonly associated with cancer, potentially neglecting genes involved in pathways that contribute to the unique phenotype of MicCRC and are not typically associated with cancer.

In conclusion, in this study, we investigated the clinical features of MicCRC. MicCRC is male predominant and tends to originate in the left side of the large intestine. In terms of prognostic factors, MicCRC was associated with high-grade differentiation, tumor budding, and PDCs. As for molecular characteristics, we recognized that MicCRC exhibited a high rate of aberrant p53 expression, proficient MMR protein expression, and a low rate of *RAS/RAF* hotspot mutations. This distinct clinicopathologic and molecular features discern MicCRC from conventional CRC.

doi:10.6342/NTU202301505

5. References

[1] Xi Y, Xu P. Global colorectal cancer burden in 2020 and projections to 2040. Transl. Oncol. 2021; 14:101174.

[2] Remo A, Fassan M, Vanoli A, et al. Morphology and molecular features of rare colorectal carcinoma histotypes. Cancers (Basel). 2019; 11:1036.

[3] Nassar H. Carcinomas with micropapillary morphology: Clinical significance and current concepts. Adv. Anat. Pathol. 2004; 11:297-303.

[4] Verdú M, Román R, Calvo M, et al. Clinicopathological and molecular characterization of colorectal micropapillary carcinoma. Mod. Pathol. 2011; 24:729-738.

[5] Guzińska Ustymowicz K. Invasive micropapillary carcinoma: A distinct type of adenocarcinomas in the gastrointestinal tract. World J Gastroenterol. 2014; 20:4597.

[6] Zhao L, Liu SY, Li YM, Xiong ZT. Villin is a biomarker for reverse polarity in colorectal micropapillary carcinoma. Oncol. Lett. 2020; 21.

[7] Cserni G. Reversed polarity of the glandular epithelial cells in micropapillary carcinoma of the large intestine and the EMA/MUC1 immunostain. Pathology. 2014; 46:527-532.

[8] Onuma K, Sato Y, Okuyama H, et al. Aberrant activation of Rho/ROCK signaling in impaired polarity switching of colorectal micropapillary carcinoma. J. Pathol. 2021; 255:84-94.

doi:10.6342/NTU202301505

[9] Guo Z, Yang Z, Li D, et al. Colorectal cancer with invasive micropapillary components (IMPCs) shows high lymph node metastasis and a poor prognosis. Medicine. 2020; 99:e20238.

[10] Lee HJ, Eom DW, Kang GH, et al. Colorectal micropapillary carcinomas are associated with poor prognosis and enriched in markers of stem cells. Mod. Pathol. 2013; 26:1123-1131.

[11] Xu F, Xu J, Lou Z, et, al. Micropapillary component in colorectal carcinoma is associated with lymph node metastasis in T1 and T2 stages and decreased survival time in TNM stages I and II. Am. J. Surg. Pathol. 2009; 33:1287-1292.

[12] Zlobec I, Lugli A. Prognostic and predictive factors in colorectal cancer. J. Clin. Pathol. 2008; 61:561-569.

[13] Kim MJ, Hong SM, Jang SJ, et al. Invasive colorectal micropapillary carcinoma: an aggressive variant of adenocarcinoma. Hum. Pathol. 2006; 37:809-815.

[14] Barresi V, Branca G, Vitarelli E, Tuccari G. Micropapillary pattern and poorly differentiated clusters represent the same biological phenomenon in colorectal cancer: A proposal for a change in terminology. Am. J. Clin. Pathol. 2014; 142:375-383.

[15] Ryan É, Khaw YL, Creavin B, et al. Tumor budding and PDC grade are stage independent predictors of clinical outcome in mismatch repair deficient colorectal cancer. Am. J. Surg. Pathol. 2018; 42:60-68.

doi:10.6342/NTU202301505

[16] Lugli A, Kirsch R, Ajioka Y, et al. Recommendations for reporting tumor budding in colorectal cancer based on the International Tumor Budding Consensus Conference (ITBCC) 2016. Mod. Pathol. 2017; 30:1299-1311.

[17] Zhang S, Zhang D, Yang Z, Zhang X. Tumor Budding, Micropapillary pattern, and polyploidy giant cancer cells in colorectal cancer: current status and future prospects. Stem Cells Int. 2016; 2016:1-8.

[18] Ueno H, Murphy J, Jass JR, Mochizuki H, Talbot IC. Tumour `budding' as an index to estimate the potential of aggressiveness in rectal cancer. Histopathology. 2002; 40:127-132.

[19] Ueno H, Kajiwara Y, Shimazaki H, Shinto E, Hashiguchi Y, Nakanishi K, Maekawa K, Katsurada Y, Nakamura T, Mochizuki H, Yamamoto J, Hase K. New Criteria for Histologic Grading of Colorectal Cancer. Am. J. Surg. Pathol. 2012:193-201.

[20] Aikawa A, Fujita H, Kosaka T, Minato H, Kiyokawa E. Clinicopathological significance of heterogeneic ezrin expression in poorly differentiated clusters of colorectal cancers. Cancer Sci. 2019; 110:2667-2675.

[21] Hong M, Kim JW, Shin MK, Kim BC. Poorly differentiated clusters in colorectal adenocarcinomas share biological similarities with micropapillary patterns as well as tumor buds. J. Korean Med. Sci. 2017; 32:1595.

[22] Harada S, Morlote D. Molecular pathology of colorectal cancer. Adv. Anat. Pathol.

doi:10.6342/NTU202301505

2020; 27:20-26.

[23] Shi Q, Shao K, Jia H, et al. Genomic alterations and evolution of cell clusters in metastatic invasive micropapillary carcinoma of the breast. Nat. Commun. 2022; 13.

[24] Guo CC, Dadhania V, Zhang L, et al. Gene expression profile of the clinically aggressive micropapillary variant of bladder cancer. Eur. Urol. 2016; 70:611-620.

[25] Muller PAJ, Vousden KH, Norman JC. P53 and its mutants in tumor cell migration and invasion. J. Cell Biol. 2011; 192:209-218.

[26] Gonzalez RS, Huh WJ, Cates JMM, et al. Micropapillary colorectal carcinoma: clinical, pathological and molecular properties, including evidence of epithelial-mesenchymal transition. Histopathology. 2017; 70:223-231.

[27] Edge SB, Compton CC. The American Joint Committee on Cancer: the 7th edition of the AJCC cancer staging manual and the future of TNM. Ann. Surg. Oncol. 2010; 17:1471-1474.

[28] Zhan T, Rindtorff N, Boutros M. Wnt signaling in cancer. Oncogene. 2017; 36:1461-1473.

[29] Kaserer K, Schmaus J, Bethge U, et al. Staining patterns of p53 immunohistochemistry and their biological signi®cance in colorectal cancer. J. Pathol. 2000;190(4):450-6..

[30] Baran B, Mert Ozupek N, Yerli Tetik N, Acar E, Bekcioglu O, Baskin Y. Difference

doi:10.6342/NTU202301505

between left-sided and right-sided colorectal cancer: a focused review of literature. Gastroenterology Res. 2018; 11:264-273.

[31] Lugli A, Zlobec I, Berger MD, Kirsch R, Nagtegaal ID. Tumour budding in solid cancers. Nat. Rev. Clin. Oncol. 2021; 18:101-115.

[32] Ueno H, Hase K, Hashiguchi Y, et al. Site-specific tumor grading system in colorectal cancer: multicenter pathologic review of the value of quantifying poorly differentiated clusters. Am. J. Surg. Pathol. 2014; 38:197-204.

[33] Alexander D, Jhala N, Chatla C, et al. High-grade tumor differentiation is an indicator of poor prognosis in African Americans with colonic adenocarcinomas. Cancer. 2005; 103:2163-2170.

[34] Shivji S, Conner JR, Barresi V, Kirsch R. Poorly differentiated clusters in colorectal cancer: a current review and implications for future practice. Histopathology. 2020; 77:351-368.

[35] Barresi V, Bonetti LR, Bettelli S. *KRAS, NRAS, BRAF* mutations and high counts of poorly differentiated clusters of neoplastic cells in colorectal cancer: observational analysis of 175 cases. Pathology. 2015; 47:551-556.

[36] Lavin MF, Gueven N. The complexity of p53 stabilization and activation. Cell Death Differ. 2006; 13:941-950.

[37] Araki K, Ebata T, Guo AK, Tobiume K, Wolf SJ, Kawauchi K. P53 regulates

doi:10.6342/NTU202301505

cytoskeleton remodeling to suppress tumor progression. Cell. Mol. Life Sci. 2015; 72:4077-4094.

[38] Powell E, Piwnica-Worms D, Piwnica-Worms H. Contribution of p53 to metastasis. Cancer Discov. 2014; 4:405-414.

[39] Ebata T, Hirata H, Kawauchi K. Functions of the tumor suppressors p53 and Rb in actin cytoskeleton remodeling. Biomed Res. Int. 2016; 2016:1-10.

[40] Oka S, Leon J, Tsuchimoto D, Sakumi K, Nakabeppu Y. MUTYH, an adenine DNA glycosylase, mediates p53 tumor suppression via PARP-dependent cell death. Oncogenesis. 2014; 3:e121.

[41] Prévostel C, Rammah-Bouazza C, Trauchessec H, et al. SOX9 is an atypical intestinal tumor suppressor controlling the oncogenic Wnt/ß-catenin signaling. Oncotarget. 2016; 7:82228-82243.

[42] Thien A, Prentzell MT, Holzwarth B, et al. TSC1 activates TGF-β-Smad2/3 signaling in growth arrest and epithelial-to-mesenchymal transition. Dev. Cell. 2015; 32:617-630.

[43] Centore RC, Sandoval GJ, Soares LMM, Kadoch C, Chan HM. Mammalian SWI/SNF chromatin remodeling complexes: emerging mechanisms and therapeutic strategies. Trends Genet. 2020; 36:936-950.

[44] Zhou Y, Rychahou P, Wang Q, Weiss HL, Evers BM. TSC2/mTORC1 signaling controls paneth and goblet cell differentiation in the intestinal epithelium. Cell Death Dis.

doi:10.6342/NTU202301505

2015; 6:e1631-e1631.

doi:10.6342/NTU202301505

6. Figure

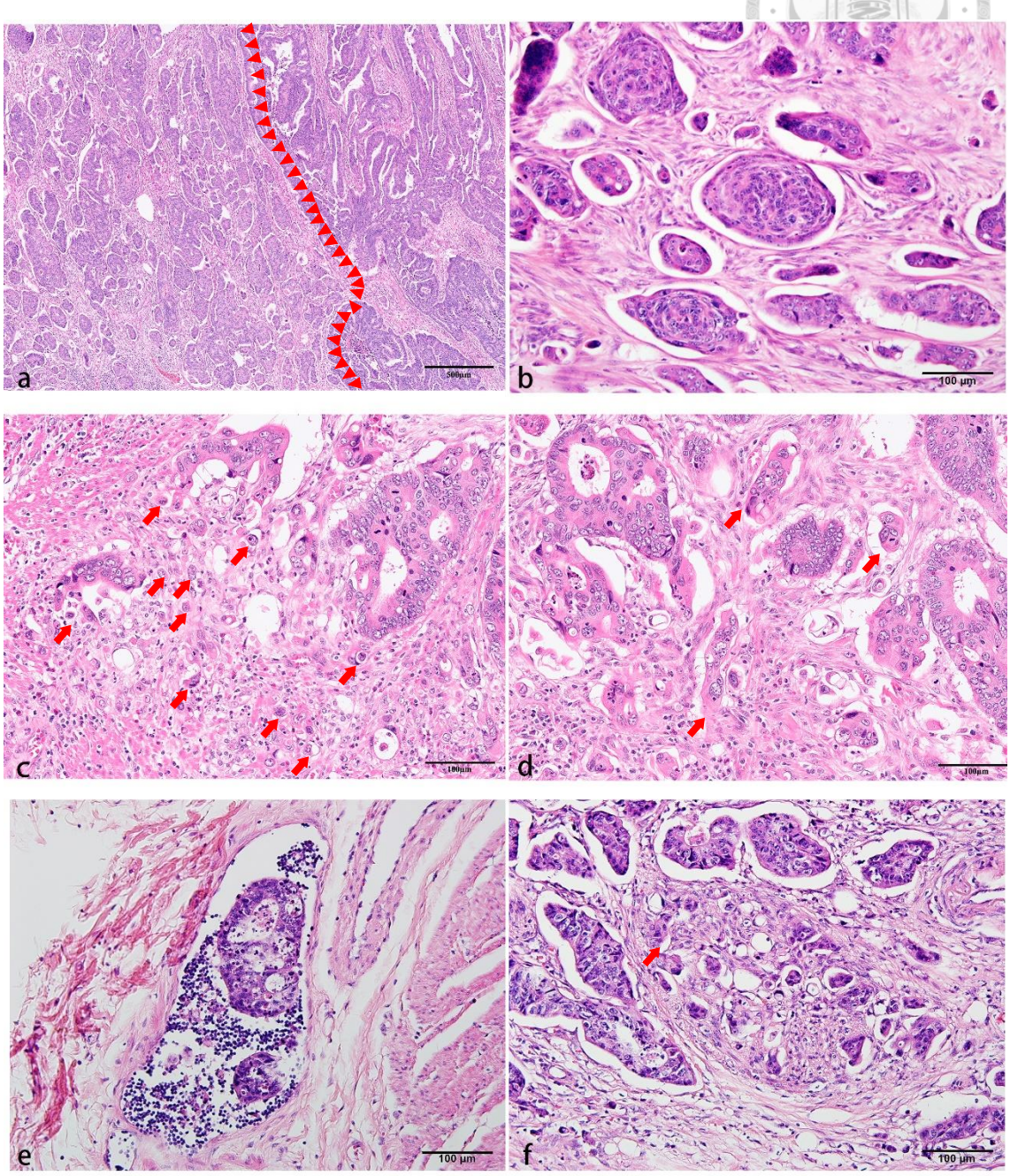

Figure 1. Morphology of MicCRC & prognosis factors

(a, b) Morphology features of MicCRC in X4 object lens (a) and X20 object lens, red arrows indicated the distinct group of micropapillary carcinoma. (c) Morphology of high-grade tumor budding in X20 object lens, red arrows indicated the clusters of tumors

doi:10.6342/NTU202301505

budding (d) Morphology of high-grade PDC in X20 object lens, red arrows indicated the clusters of PDC (e) Presence of lymphovascular invasion in X20 object lens (f) Presence of perineural invasion in X20 object lens, red arrows indicated the perineural invasion.

doi:10.6342/NTU202301505

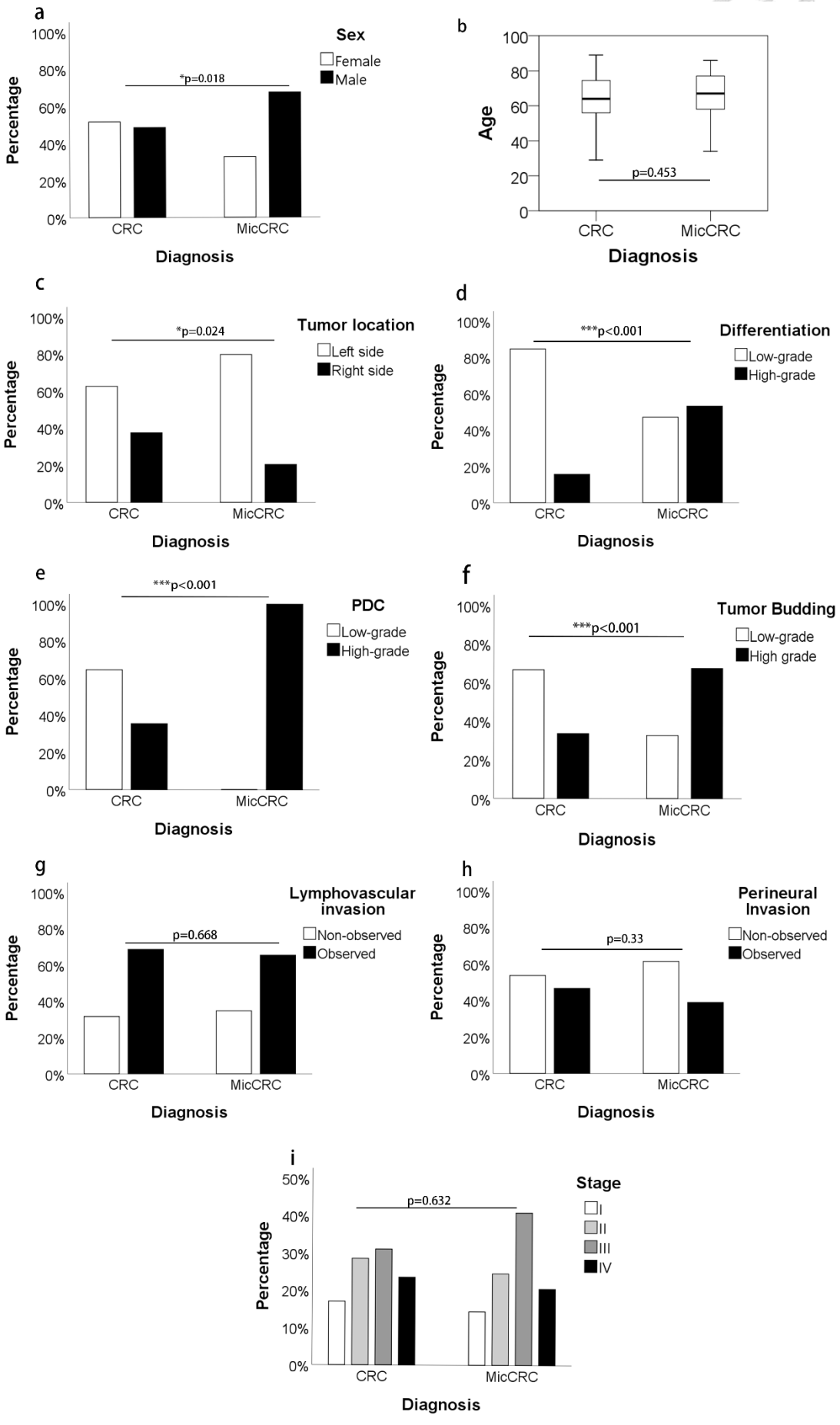

doi:10.6342/NTU202301505

Figure 2. Comparison of clinicopathology features between CRCs and MicCRCs

(a- i) Comparison of sex (a), age (b), tumor location (c), differentiation (d), PDC (e), tumor budding (f), lymphovascular invasion (g), perineural invasion (h), and stage (i) between CRC and MicCRC (* indicates $P < 0.05$, *** indicates $P < 0.001$)

doi:10.6342/NTU202301505

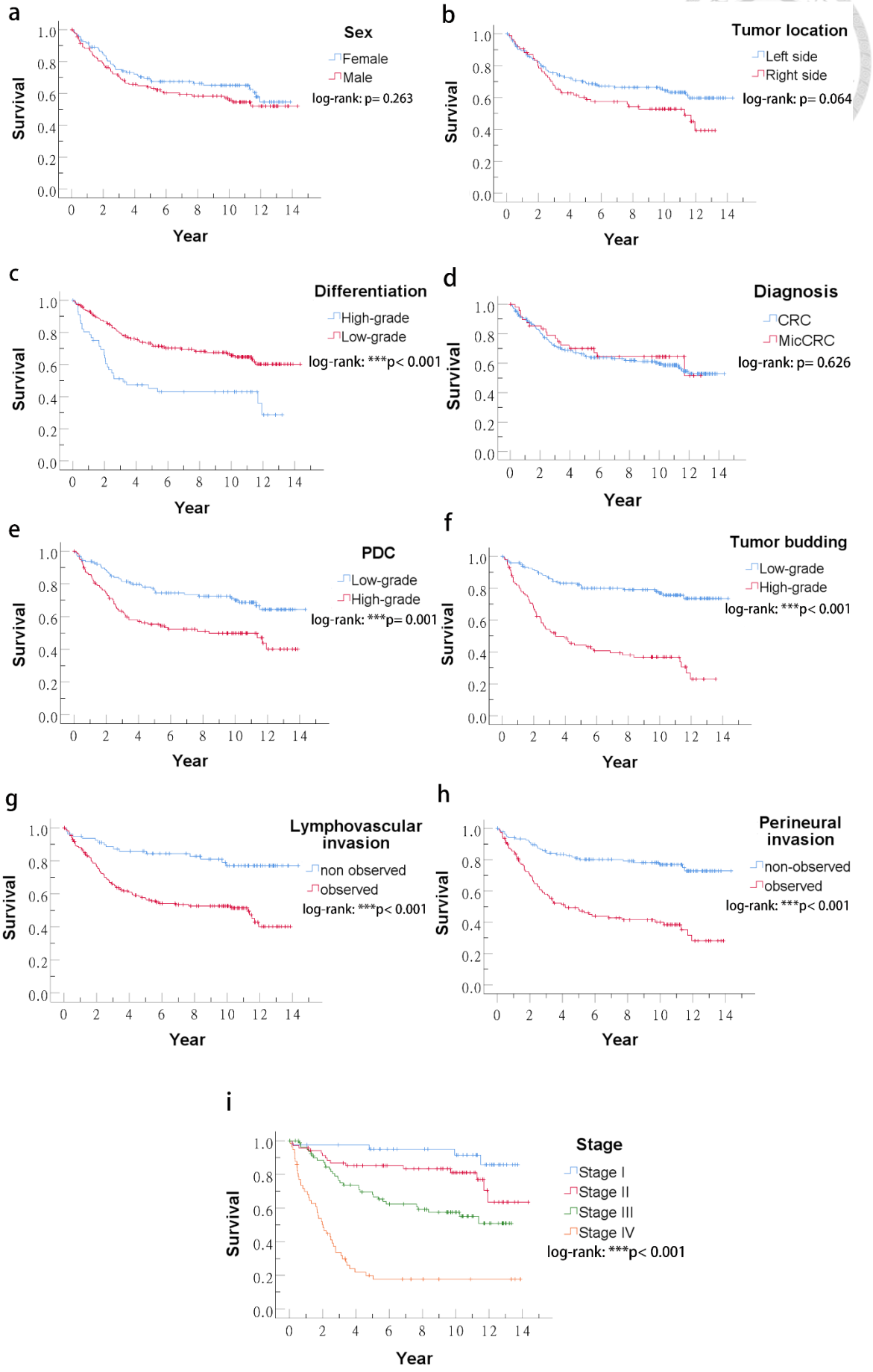

doi:10.6342/NTU202301505

Figure 3. Univariate survival analysis of different prognosis factors.

(a-i) Kaplan–Meier overall survival rate of sex (a), age (b), tumor location (c), differentiation (d), PDC (e), tumor budding (f), lymphovascular invasion (g), perineural invasion (h), and stage (i) (* indicates $P < 0.05$, *** indicates $P < 0.001$).

doi:10.6342/NTU202301505

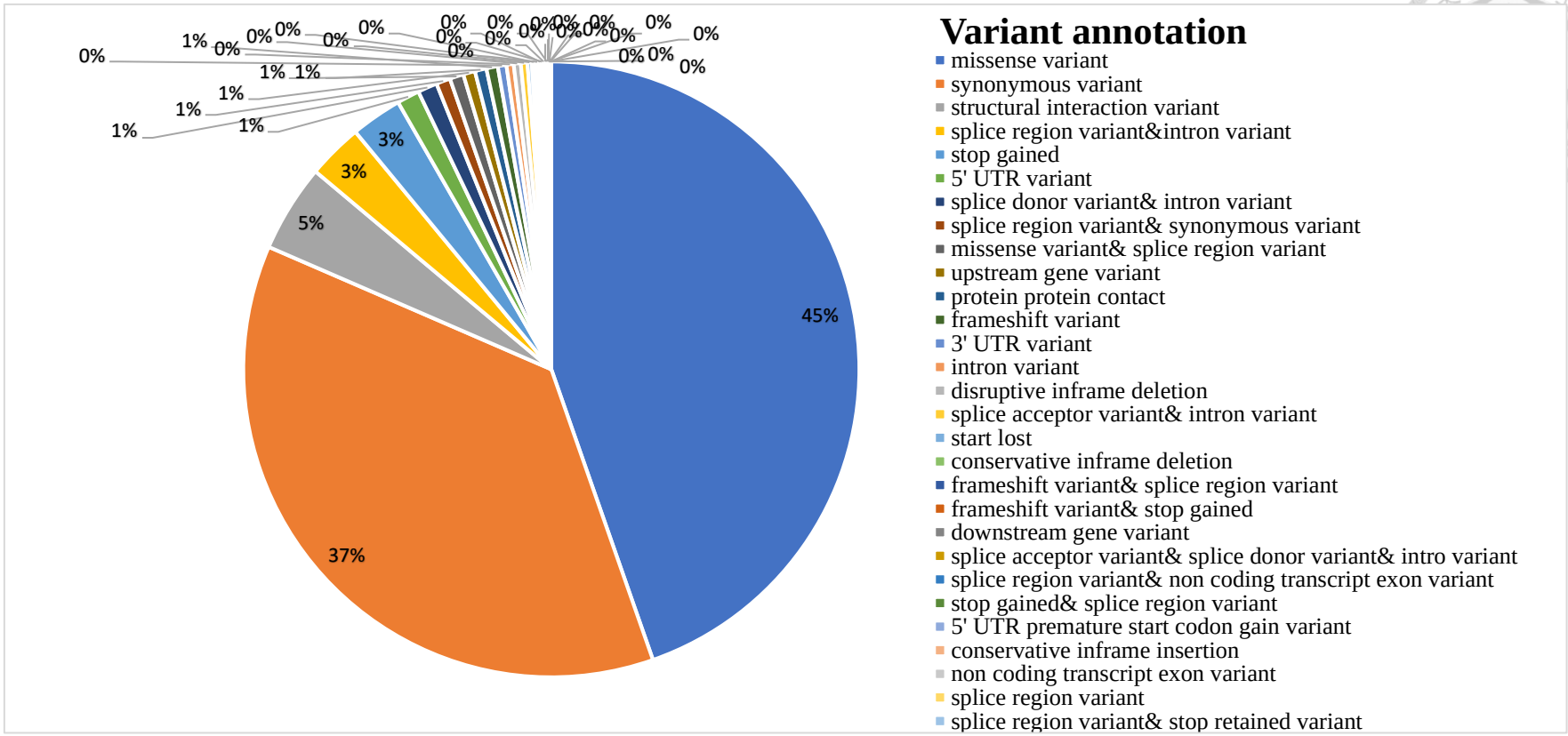

Figure 4. Overview of gene annotation of NGS (n=12)

Gene annotation analysis of NGS through QIAseq Comprehensive Cancer Panel. The variant annotations are organized in descending order based on their frequency in all NGS results.

doi:10.6342/NTU202301505

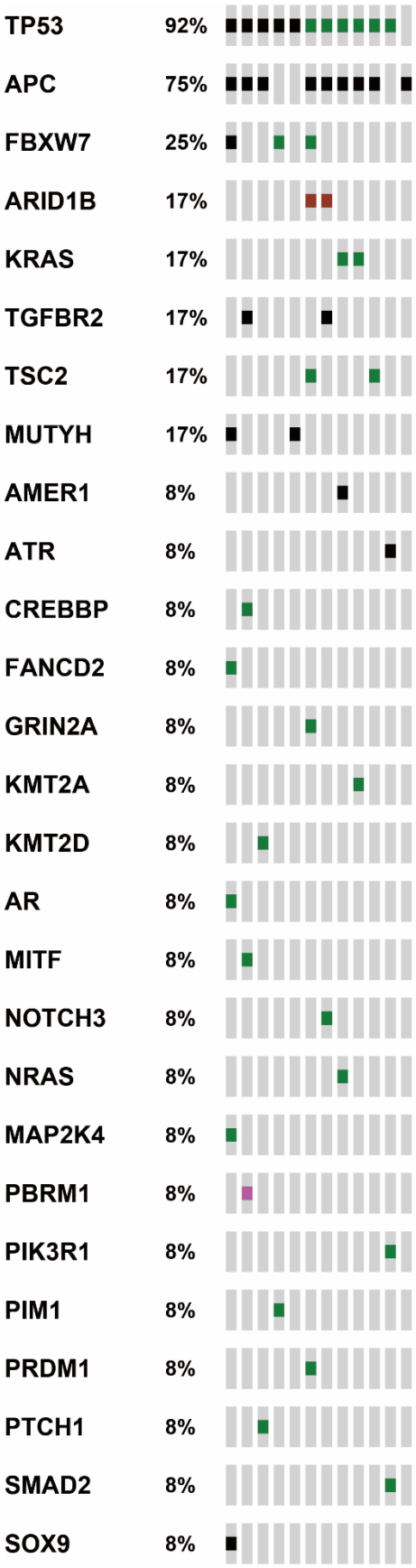

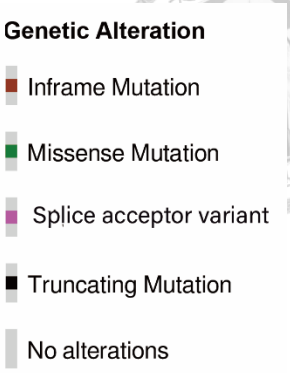

doi:10.6342/NTU202301505

Figure 5. Gene alteration of MicCRC (n=12)

An overview of the altered genes in MicCRC has been conducted following validation through Sanger sequencing and IHC. For a detailed description of the alterations, please refer to Supplementary Table 3.

doi:10.6342/NTU202301505

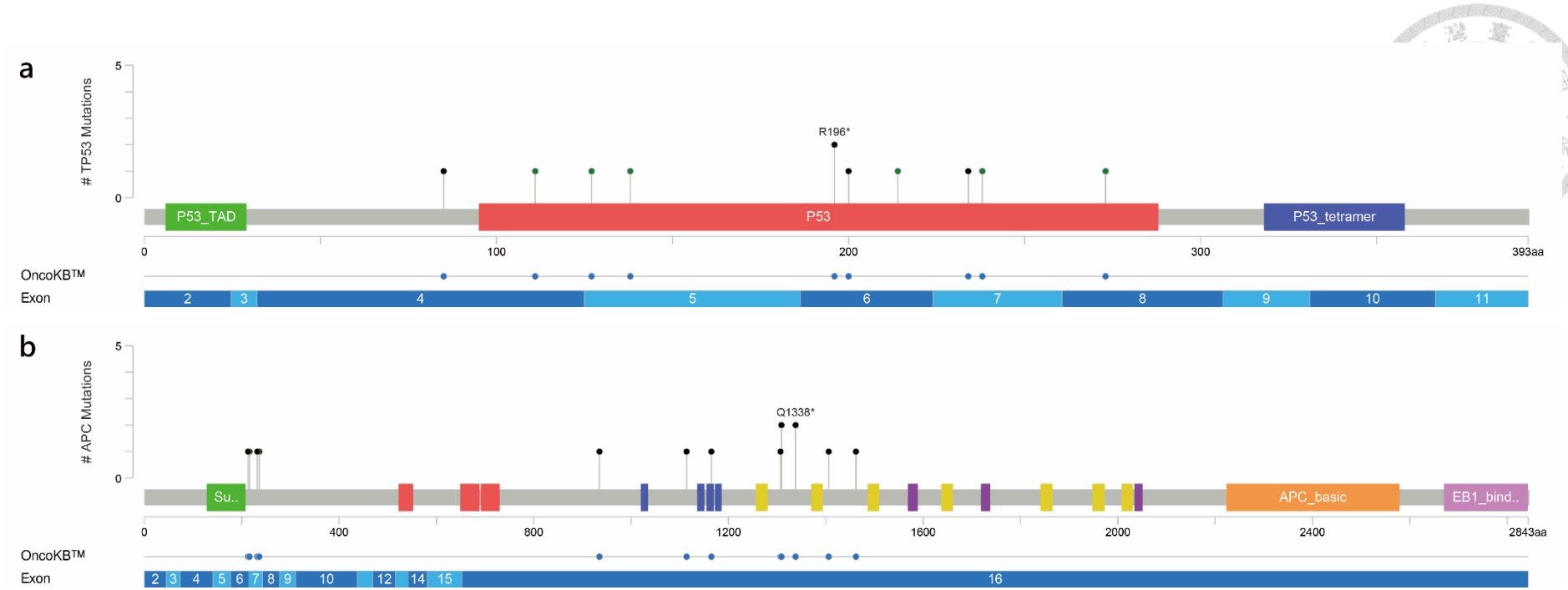

Figure 6. Mutation mapper of mutated genes

(a) Mutation mapper of *APC* gene (b) Mutation mapper of *TP53* gene. The mutation database was generated using the cBioPortal Mutation Mapper tool (https://www.cbioportal.org/mutation_mapper).

doi:10.6342/NTU202301505

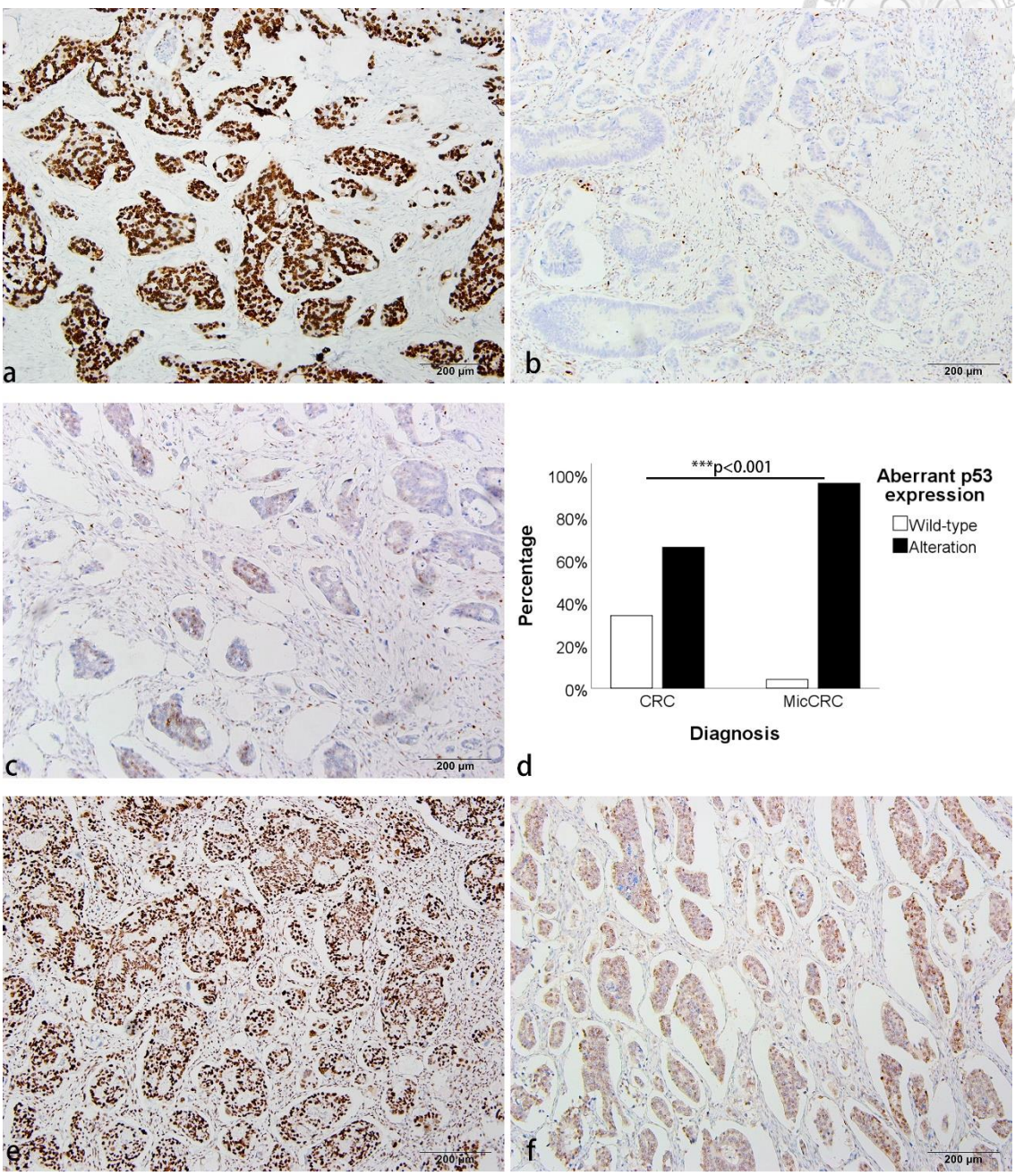

Figure 7. IHC results of MicCRC.

(a) P53 overexpression in MicCRC in X10 object lens. (b) P53 loss in MicCRC in × 10 object lens. (c) Wild type P53 expression in MicCRC in X10 object lens. (d) Comparison of p53 aberrant expression between CRC and MicCRC (*** indicate P <

doi:10.6342/NTU202301505

0.001). (e) MSH6 expression is preserved in MicCRC in X10 object lens. (f) PMS2 expression is preserved in MicCRC in X10 object lens.

doi:10.6342/NTU202301505

7. Table

Table 1. Clinicopathological features of MicCRC.

Table 1. Clinicopathological features of MicCRC.

Clinical features	Number, n= 49 (%)
Sex (male)	33 (67%)
Age (mean, range)	66 (34-86)
Tumor location	
Right colon	10 (20%)
Left colon	39 (80%)
Prognosis Feature	
Differentiation (High-grade)	26(53%)
Poorly differentiated clusters (High-grade)	49(100%)
Tumor Budding (High-grade)	33(67%)
Lymphovascular invasion	32(65%)
Perineural invasion	19(39%)
TNM anatomical Stage I	7(14%)
TNM anatomical Stage II	12(39%)
TNM anatomical Stage III	20(41%)
TNM anatomical Stage IV	10(20%)

doi:10.6342/NTU202301505

Table 2. Correlation between clinicopathological between MicCRC and CRC.

Table 2. Correlation between clinicopathological between MicCRC and CRC.

Features	MicCRC, n=49	CRC, n=200	P value
Sex (male)	33 (67%)	97(49%)	0.018
Age (mean)	65.9 (±12.6)	64.4(±12.4)	0.453
Tumor location			0.024
Right colon	10 (20%)	75(38%)	
Left colon	39 (80%)	125(63%)	
Prognosis Feature			
Differentiation (High-grade)	26(53%)	31(16%)	<0.001
Poorly differentiated clusters (High-grade)	49(100%)	71(36%)	<0.001
Tumor Budding (High-grade)	33(67%)	67(34%)	<0.001
Lymphovascular invasion	32(65%)	137(69%)	0.668
Perineural invasion	19(39%)	93(47%)	0.33
TNM Stage			0.632
TNM anatomical Stage I	7(14%)	34(17%)	
TNM anatomical Stage II	12(39%)	57(29%)	
TNM anatomical Stage III	20(41%)	62(31%)	
TNM anatomical Stage IV	10(20%)	47(24%)	

doi:10.6342/NTU202301505

Table 3. Survival analysis of MicCRC.

Table 3. Survival analysis of MicCRC.

Features	Univariate analysis		Multivariate analysis	
	HR (95% CI)	*P* value	HR (95% CI)	*P* value
Sex-Male	1.256(0.843-1.873)	0.263	1.003(0.661-1.524)	0.987
Age	1.027(1.010-1.045)	0.002	1.031(1.013-1.050)	0.001
Diagnosis-Micropapillary	0.867(0.514-1.463)	0.593	0.479(0.258-0.888)	0.02
Differentiation-High grade	2.326 (1.528-3.543)	<0.001	2.420(1.451-4.035)	0.001
Poorly differentiated clusters	2.061(1.371-3.098)	0.001	0.718(0.419-1.231)	0.228
Tumor budding-High grade	4.149 (2.720-6.328)	<0.001	3.280(1.924-5.591)	<0.001
Lymphovascular invasion	3.140 (1.834-5.376)	<0.001	0.906(0.482-1.703)	0.759
Perineural invasion	3.697(2.407-5.677)	<0.001	1.999(1.224-3.266)	0.006
Anatomical stage		<0.001		<0.001
I	0.049 (0.018-0.137)		0.085(0.028-0.261)	
II	0.126 (0.069-0.227)		0.120(0.062-0.232)	
III	0.270 (0.171-0.426)		0.218(0.133-0.356)	
IV	—		—	

doi:10.6342/NTU202301505

Table 4. Molecular features of MicCRC

Table 4. Molecular features of MicCRC.	
IHC staining	Number, n= 49 (%)
Aberrant P53 expression	47(96%)
MMR expression	49(100%)
Mutations	Number, n=49
KRAS/NRAS	10(20%)
BRAF	2(4%)

doi:10.6342/NTU202301505

Table 5. *RAS/RAF* mutation in MicCRC

Diagnosis	Genes	Exon	Nucleotide change	Protein change
MicCRC	*KRAS*	E2	c.38G>A	p. Gly13Asp
MicCRC	*KRAS*	E2	c.35G>A	p. Gly12Asp
MicCRC	*KRAS*	E2	c.35G>T	p. Gly12Val
MicCRC	*KRAS*	E2	c.35G>A	p. Gly12Asp
MicCRC	*KRAS*	E2	c.35G>T	p. Gly12Val
MicCRC	*KRAS*	E2	c.38G>A	p. Gly13Asp
MicCRC	*KRAS*	E2	c.35G>T	p. Gly12Val
MicCRC	*KRAS*	E2	c.35G>T	p. Gly12Val
MicCRC	*KRAS*	E2	c.35G>A	p. Gly12Asp
MicCRC	*KRAS*	E2	c.35G>A	p. Gly12Asp
	NRAS	E2	c.35G>T	p. Gly12Val
MicCRC	*BRAF*	E15	c.1799T>A	p. Val600Glu
MicCRC	*BRAF*	E15	c.1780G>A	p. Asp594Asn

doi:10.6342/NTU202301505

8. Supplementary table

Supplementary table 1. Targeting genes included in QIAseq Comprehensive Cancer Panel

Supplementary Table 1. Targeting genes included in QIAseq Comprehensive Cancer Panel									
ABL1	*BIRC3*	*CREBBP*	*EZH2*	*GNAS*	*KMT2C*	*NF1*	*POLE*	*SMARCB1*	*WT1*
ACVR1B	*BLM*	*CRLF2*	*FAM175A*	*GREM1*	*KMT2D*	*NF2*	*PPM1D*	*SMC1A*	*XPO1*
AKT1	*BRAF*	*CSF1R*	*FAM46C*	*GRIN2A*	*KRAS*	*NFE2L2*	*PPP2R1A*	*SMC3*	*XRCC2*
AKT2	*BRCA1*	*CSF3R*	*FANCA*	*H3-3A*	*LRP1B*	*NFKBIA*	*PRDM1*	*SMO*	*XRCC3*
AKT3	*BRCA2*	*CTCF*	*FANCC*	*H3C2*	*MAP2K1*	*NKX2-1*	*PRKAR1A*	*SOCS1*	*ZNF217*
ALK	*BRIP1*	*CTNNA1*	*FANCD2*	*HGF*	*MAP2K2*	*NOTCH1*	*PRKDC*	*SOX2*	*ZRSR2*
AMER1	*BTK*	*CTNNB1*	*FANCE*	*HNF1A*	*MAP2K4*	*NOTCH2*	*PRSS1*	*SOX9*	
APC	*CALR*	*CUX1*	*FANCF*	*HOXB13*	*MAP3K1*	*NOTCH3*	*PTCH1*	*SPOP*	
AR	*CARD11*	*CXCR4*	*FANCG*	*HRAS*	*MAP3K14*	*NPM1*	*PTEN*	*SRC*	
ARAF	*CBL*	*CYLD*	*FAS*	*HSP90AA1*	*MAPK1*	*NRAS*	*PTPN11*	*SRSF2*	
ARID1A	*CBLB*	*DAXX*	*FBXW7*	*ID3*	*MCL1*	*NSD1*	*RAC1*	*STAG2*	
ARID1B	*CBLC*	*DDR2*	*FGF4*	*IDH1*	*MDM2*	*NSD2*	*RAD21*	*STAT3*	
ARID2	*CCND1*	*DICER1*	*FGF6*	*IDH2*	*MDM4*	*NTRK1*	*RAD50*	*STK11*	
ASXL1	*CCND3*	*DNM2*	*FGFR1*	*IGF1R*	*MED12*	*NTRK2*	*RAD51*	*SUFU*	
ATM	*CCNE1*	*DNMT3A*	*FGFR2*	*IKZF1*	*MEF2B*	*NTRK3*	*RAF1*	*SUZ12*	
ATR	*CD274*	*DOT1L*	*FGFR3*	*IKZF3*	*MEN1*	*PAK3*	*RB1*	*TAL1*	
ATRX	*CD79A*	*EED*	*FGFR4*	*IL7R*	*MET*	*PALB2*	*RET*	*TCF3*	
AURKA	*CD79B*	*EGFR*	*FH*	*INHBA*	*MITF*	*PAX5*	*RHEB*	*TERT*	

doi:10.6342/NTU202301505

AURKB	*CDC73*	*EGLN1*	*FLCN*	*IRF4*	*MLH1*	*PBRM1*	*RHOA*	*TET2*	
AURKC	*CDH1*	*EP300*	*FLT3*	*JAK1*	*MPL*	*PDGFRA*	*RIT1*	*TGFBR2*	
AXIN1	*CDK12*	*EPAS1*	*FLT4*	*JAK2*	*MRE11*	*PDGFRB*	*RNF43*	*TNFAIP3*	
AXIN2	*CDK4*	*EPHA3*	*FOXL2*	*JAK3*	*MSH2*	*PHF6*	*ROS1*	*TNFRSF14*	
B2M	*CDK6*	*EPHA5*	*FUBP1*	*KAT6A*	*MSH6*	*PIK3CA*	*RUNX1*	*TP53*	
BAP1	*CDKN2A*	*ERBB2*	*GALNT12*	*KDM5C*	*MTOR*	*PIK3R1*	*SDHB*	*TRAF3*	
BCL2	*CDKN2B*	*ERBB3*	*GATA1*	*KDM6A*	*MUTYH*	*PIK3R2*	*SETBP1*	*TSC1*	
BCL2L1	*CDKN2C*	*ERBB4*	*GATA2*	*KDR*	*MYC*	*PIM1*	*SETD2*	*TSC2*	
BCL6	*CEBPA*	*ERG*	*GATA3*	*KEAP1*	*MYCL*	*PLCG1*	*SF3B1*	*TSHR*	
BCOR	*CHEK1*	*ESR1*	*GEN1*	*KIT*	*MYCN*	*PMS1*	*SMAD2*	*U2AF1*	
BCORL1	*CHEK2*	*ETV6*	*GNA11*	*KMT2A*	*MYD88*	*PMS2*	*SMAD4*	*U2AF2*	
BCR	*CIC*	*EXO1*	*GNAQ*	*KMT2B*	*Name*	*POLD1*	*SMARCA4*	*VHL*	

doi:10.6342/NTU202301505

Supplementary table 2. Sanger sequencing primer

Gene name	Primer sequence (5'-3')
KRAS	
Exon 2 F	AGGTACTGGTGGAGTATTTGA
Exon 2 R	TGTATCAAAGAATGGTCCTGC
NRAS	
Exon 2 F	GGCTCGCCAATTAACCCTGAT
Exon 2 R	CGACAAGTGAGAGACAGGAT
BRAF	
Exon 15 F	TCATAATGCTTGCTCTGATAGGA
Exon 15 R	GGCCAAAAATTTAATCAGTGGA
TP53	
Exon 4 F1	TGCTCTTTTCACCCATCTAC
Exon 4 R1	ATACGGCCAGGCATTGAAGT
Exon 4 F2	TGCACCAGCAGCTCCTACAC
Exon 4 R2	CCCAAAGTTCCAAACAAAAGA
Exon 5 F	GTTTCTTTGCTGCCGTCTTC
Exon 5 R	ACCCTGGGCAACCAGCCCTGT
Exon 6 F	TGGTTGCCCAGGGTCCCCAG
Exon 6 R	GGAGGGCCACTGACAACCA
Exon 7 F	CTTGCCACAGGTCTCCCCAA
Exon 7 R	AGGGGTCAGAGGCAAGCAGA
Exon 8+9 F	GGTGGTTGGGAGTAGATGGA
Exon 8+9 R	AAGAAAACGGCATTTTGAGTG

doi:10.6342/NTU202301505

Supplementary table 3. Variants details of the mutated genes.

Sample	Chromosome	Function	Annotation	Gene	Exon	Nucleotide change	Protein change
N35	chrX	exonic	stop gained	*AMER1*	E2	c.1096C>T	p. Gln366*
N31	chr5	exonic	stop gained	*APC*	E16	c.3340C>T	p. Arg1114*
N31	chr5	exonic	stop gained	*APC*	E16	c.4216C>T	p. Gln1406*
N33	chr5	exonic	stop gained	*APC*	E16	c.4012C>T	p. Gln1338*
N33	chr5	exonic	stop gained	*APC*	E6	c.637C>T	p. Arg213*
N34	chr5	exonic	stop gained	*APC*	E7	c.694C>T	p. Arg232*
N34	chr5	splicing	stop gained &splice region variant	*APC*	E7	c.646C>T	p. Arg216*
N35	chr5	exonic	frameshift variant	*APC*	E16	c.4393_4394dupAG	p. Ser1465fs
N36	chr5	exonic	stop gained	*APC*	E16	c.2805C>G	p. Tyr935*
N36	chr5	exonic	stop gained	*APC*	E16	c.4012C>T	p. Gln1338*
N37	chr5	exonic	stop gained	*APC*	E7	c.706C>T	p. Gln236*
N45	chr5	exonic	stop gained	*APC*	E16	c.3493A>T	p. Lys1165*
N52	chr5	exonic	frameshift variant	*APC*	E16	c.3929delA	p. Lys1310fs
N54	chr5	exonic	frameshift variant	*APC*	E16	c.3927_3931delAAAGA	p. Glu1309fs
N54	chr5	exonic	stop gained	*APC*	E16	c.3925G>T	p. Glu1309*
N52	chrX	exonic	missense variant	*AR*	E1	c.173A>T	p. Gln58Leu
N31	chr6	exonic	disruptive inframe deletion	*ARID1B*	E1	c.980_985delGAGGAG	p. Gly327_Gly328del
N54	chr6	exonic	disruptive inframe insertion	*ARID1B*	E1	c.360_362dupGCA	p. Gln121dup
N38	chr3	exonic	frameshift variant	*ATR*	E10	c.2320delA	p. Ile774fs
N37	chr16	exonic	missense variant	*CREBBP*	E14	c.2849C>T	p. Thr950Met
N52	chr3	exonic	missense variant	*FANCD2*	E25	c.2336G>A	p. Arg779His
N31	chr4	exonic	missense variant	*FBXW7*	E10	c.1436G>A	p. Arg479Gln
N51	chr4	exonic	missense variant	*FBXW7*	E12	c.1931G>T	p. Gly644Val
N52	chr4	exonic	missense variant	*FBXW7*	E10	c.1513C>T	p. Arg505Cys

doi:10.6342/NTU202301505

Sample	Chromosome	Function	Annotation	Gene	Exon	Nucleotide change	Protein change
N52	chr4	exonic	stop gained	*FBXW7*	E12	c.1922C>G	p. Ser641*
N31	chr16	exonic	missense variant	*GRIN2A*	E12	c.2456G>A	p. Gly819Asp
N45	chr11	exonic	missense variant	*KMT2A*	E27	c.9566T>C	p. Ile3189Thr
N33	chr12	exonic	missense variant	*KMT2D*	E34	c.9268G>A	p. Glu3090Lys
N33	chr12	exonic	missense variant	*KMT2D*	E6	c.730T>A	p. Cys244Ser
N35	chr12	exonic	missense variant	*KRAS*	E2	c.35G>A	p. Gly12Asp
N45	chr12	exonic	missense variant	*KRAS*	E2	c.35G>A	p. Gly12Asp
N52	chr17	exonic	missense variant	*MAP2K4*	E5	c.433C>T	p. Arg145Trp
N37	chr3	exonic	missense variant	*MITF*	E10	c.1199G>A	p. Arg400Gln
N52	chr1	exonic	stop gained	*MUTYH*	E2	c.90G>A	p. Trp30*
N55	chr1	exonic	stop gained	*MUTYH*	E2	c.90G>A	p. Trp30*
N54	chr19	exonic	missense variant	*NOTCH3*	E22	c.3568C>T	p. Arg1190Cys
N35	chr1	exonic	missense variant	*NRAS*	E2	c.35G>T	p. Gly12Val
N37	chr3	splicing	splice acceptor variant& intron variant	*PBRM1*	E6	c.715-1G>T	
N38	chr5	exonic	missense variant	*PIK3R1*	E12	c.1703C>T	p. Pro568Leu
N51	chr6	exonic	missense variant	*PIM1*	E4	c.403G>A	p. Glu135Lys
N31	chr6	exonic	missense variant	*PRDM1*	E2	c.239A>T	p. Glu80Val
N33	chr9	exonic	missense variant	*PTCH1*	E12	c.1688C>T	p. Ala563Val
N38	chr18	exonic	structural interaction variant	*SMAD2*	E8	c.992A>T	p. His331Leu
N52	chr17	exonic	stop gained	*SOX9*	E3	c.886C>T	p. Gln296*
N37	chr3	exonic	frameshift variant	*TGFBR2*	E4	c.458delA	p. Lys153fs
N54	chr3	exonic	frameshift variant	*TGFBR2*	E4	c.458delA	p. Lys153fs
N31	chr17	exonic	structural interaction variant	*TP53*	E5	c.380C>A	p. Ser127Phe
N33	chr17	exonic	stop gained	*TP53*	E6	c.586C>T	p. Arg196*
N35	chr17	exonic	structural interaction variant	*TP53*	E5	c.413C>T	p. Ala138Val

doi:10.6342/NTU202301505

Sample	Chromosome	Function	Annotation	Gene	Exon	Nucleotide change	Protein change
N36	chr17	exonic	structural interaction variant	*TP53*	E6	c.641A>G	p. His214Arg
N37	chr17	exonic	frameshift variant	*TP53*	E6	c.599dupA	p. Asn200fs
N38	chr17	exonic	missense variant	*TP53*	E4	c.332T>C	p. Leu111Pro
N45	chr17	exonic	structural interaction variant	*TP53*	E8	c.818G>A	p. Arg273His
N51	chr17	exonic	stop gained	*TP53*	E7	c.702C>A	p. Tyr234*
N52	chr17	exonic	stop gained	*TP53*	E6	c.586C>T	p. Arg196*
N54	chr17	exonic	structural interaction variant	*TP53*	E7	c.713G>A	p. Cys238Tyr
N55	chr17	exonic	frameshift variant& missense variant	*TP53*	E4	c.253_254delCCinsT	p. Pro85fs
N31	chr16	exonic	missense variant	*TSC2*	E16	c.1696G>A	p. Gly566Arg
N36	chr16	exonic	missense variant	*TSC2*	E22	c.2366T>C	p. Val789Ala

doi:10.6342/NTU202301505

Supplementary table 4. Variants details of the uncertain genes.

Sample	Chromosome	Function	Annotation	Gene	Exon	Nucleotide change	Protein change
N33	chr9	exonic	stop gained	*ABL1*	E4	c.840G>A	p. Trp280*
N34	chr2	splicing	splice donor variant& intron variant	*ALK*	E28	c.4164+1G>A	
N54	chr2	exonic	missense variant	*ALK*	E29	c.4307G>A	p. Arg1436His
N52	chr11	exonic	missense variant	*ATM*	E58	c.8450A>G	p. Tyr2817Cys
N31	chr3	exonic	missense variant	*ATR*	E3	c.164T>A	p. Leu55His
N36	chrX	exonic	missense variant	*ATRX*	E16	c.4604C>T	p. Thr1535Ile
N45	chr13	exonic	missense variant	*BRCA2*	E11	c.4372C>T	p. His1458Tyr
N54	chr7	intronic	downstream gene variant	*CARD11*		c.*437G>A	
N31	chr19	exonic	missense variant	*CIC*	E11	c.5408C>T	p. Ser1803Phe
N31	chr7	exonic	missense variant	*EGFR*	E1	c.19G>A	p. Ala7Thr
N33	chr2	exonic	disruptive inframe deletion	*EPAS1*	E10	c.1329_1331delGAG	p. Arg443del
N52	chr17	exonic	missense variant	*ERBB2*	E15	c.1796G>A	p. Arg599His
N54	chr12	exonic	missense variant	*ERBB3*	E27	c.3380G>A	p. Arg1127His
N55	chr2	exonic	missense variant	*ERBB4*	E24	c.2936G>A	p. Arg979Gln
N33	chr8	exonic	missense variant	*FGFR1*	E4	c.403G>A	p. Val135Ile
N31	chr13	exonic	missense variant	*FLT3*	E12	c.1582C>T	p. Leu528Phe
N45	chr5	exonic	missense variant	*FLT4*	E30	c.4061G>A	p. Arg1354His
N35	chr3	exonic	missense variant	*GATA2*	E5	c.1024G>A	p. Ala342Thr
N55	chr15	exonic	structural interaction variant	*IGF1R*	E17	c.3255C>T	p. Leu1086Phe
N52	chr8	exonic	missense variant	*KAT6A*	E17	c.4441A>G	p. Ser1481Gly
N52	chr8	exonic	missense variant	*KAT6A*	E9	c.1492G>A	p. Val498Met
N54	chrX	exonic	missense variant	*KDM6A*	E6	c.515G>C	p. Arg172Pro
N52	chr4	exonic	structural interaction variant	*KDR*	E20	c.2736C>T	

doi:10.6342/NTU202301505

Sample	Chromosome	Function	Annotation	Gene	Exon	Nucleotide change	Protein change
N36	chr19	exonic	missense variant	*KMT2B*	E37	c.7978T>C	
N31	chr7	exonic	missense variant	*KMT2C*	E7	c.925C>T	p. Pro309Ser
N33	chr7	exonic	stop gained	*KMT2C*	E14	c.2263C>T	p. Gln755*
N34	chr7	exonic	missense variant	*KMT2C*	E7	c.925C>T	p. Pro309Ser
N35	chr7	exonic	missense variant	*KMT2C*	E7	c.925C>T	p. Pro309Ser
N38	chr7	exonic	missense variant	*KMT2C*	E7	c.925C>T	p. Pro309Ser
N45	chr7	exonic	missense variant	*KMT2C*	E7	c.925C>T	p. Pro309Ser
N51	chr7	exonic	stop gained	*KMT2C*	E14	c.2263C>T	p. Gln755*
N51	chr7	exonic	missense variant	*KMT2C*	E7	c.925C>T	p. Pro309Ser
N52	chr7	exonic	stop gained	*KMT2C*	E14	c.2263C>T	p. Gln755*
N52	chr7	exonic	missense variant	*KMT2C*	E7	c.925C>T	p. Pro309Ser
N55	chr7	exonic	stop gained	*KMT2C*	E14	c.2263C>T	p. Gln755*
N33	chr2	exonic	missense variant	*LRP1B*	E10	c.1529G>A	p. Gly510Glu
N31	chr1	exonic	missense variant	*MDM4*	E5	c.358A>G	p. Lys120Glu
N33	chr1	exonic	missense variant	*MDM4*	E9	c.812G>A	p. Ser271Asn
N52	chr7	exonic	frameshift variant	*MET*	E19	c.3704_3705delCA	p. Thr1235fs
N54	chr2	exonic	missense variant	*MSH6*	E10	c.4068G>T	p. Leu1356Phe
N52	chr2	exonic	missense variant	*MYCN*	E2	c.550G>T	p. Ala184Ser
N31	chr9	exonic	missense variant	*NOTCH1*	E23	c.3743T>C	p. Val1248Ala
N31	chr1	exonic	missense variant	*NOTCH2*	E4	c.590C>T	p. Thr197Ile
N31	chr1	exonic	missense variant	*NOTCH2*	E34	c.6126G>A	p. Met2042Ile
N33	chr1	exonic	missense variant	*NOTCH2*	E4	c.590C>T	p. Thr197Ile
N31	chr19	exonic	missense variant	*NOTCH3*	E11	c.1630C>T	p. Arg544Cys

doi:10.6342/NTU202301505

Sample	Chromosome	Function	Annotation	Gene	Exon	Nucleotide change	Protein change
N33	chr19	exonic	missense variant	*NOTCH3*	E24	c.4189G>C	p. Gly1397Arg
N37	chr19	exonic	missense variant	*NOTCH3*	E10	c.1555G>A	p. Gly519Ser
N52	chr19	exonic	missense variant	*NOTCH3*	E33	c.6696G>T	p. Lys2232Asn
N54	chr19	exonic	missense variant	*NOTCH3*	E22	c.3568C>T	p. Arg1190Cys
N31	chr5	exonic	missense variant	*NSD1*	E23	c.7417C>T	p. His2473Tyr
N35	chr15	exonic	missense variant	*NTRK3*	E16	c.1969C>G	p. Leu657Val
N45	chr15	exonic	missense variant	*NTRK3*	E7	c.755A>G	p. Asn252Ser
N36	chrX	exonic	missense variant	*PAK3*	E2	c.207G>T	p. Glu69Asp
N31	chr3	splicing	splice acceptor variant& intron variant	*PBRM1*	E13	c.1542-2A>G	
N33	chr5	exonic	structural interaction variant	*PDGFRB*	E3	c.136G>A	p. Val46Ile
N34	chr3	exonic	missense variant	*PIK3CA*	E18	c.2519C>T	p. Ser840Leu
N54	chr3	exonic	missense variant	*PIK3CA*	E2	c.334A>T	p. Ile112Phe
N51	chr7	exonic	missense variant	*PRSS1*	E2	c.107C>G	p. Pro36Arg
N55	chr7	exonic	missense variant	*PRSS1*	E4	c.452C>T	p. Thr151Met
N55	chr17	exonic	missense variant	*RNF43*	E7	c.766C>T	p. Arg256Trp
N31	chr6	exonic	missense variant	*ROS1*	E30	c.4932G>C	p. Trp1644Cys
N36	chr6	exonic	missense variant	*ROS1*	E24	c.3716A>T	p. Tyr1239Phe
N36	chr6	exonic	missense variant	*ROS1*	E42	c.6639C>A	p. Asp2213Glu
N34	chr22	splicing	splice acceptor variant& intron variant	*SMARCB1*	E2	c.206-2A>G	
N34	chr22	splicing	splice donor variant& intron variant	*SMARCB1*	E6	c.822+1G>C	
N38	chr22	splicing	splice donor variant& intron variant	*SMARCB1*	E8	c.1145+2T>C	
N38	chr22	splicing	splice donor variant& intron variant	*SMARCB1*	E6	c.822+1G>C	
N51	chr22	splicing	splice donor variant& intron variant	*SMARCB1*	E6	c.822+1G>C	

doi:10.6342/NTU202301505

Sample	Chromosome	Function	Annotation	Gene	Exon	Nucleotide change	Protein change
N52	chr7	exonic	missense variant	*SMO*	E10	c.1789G>A	p. Asp597Asn
N33	chr20	exonic	missense variant	*SRC*	E3	c.306C>A	p. Asp102Glu
N33	chr17	exonic	missense variant	*SUZ12*	E1	c.101C>G	p. Ala34Gly
N52	chr1	exonic	missense variant	*TAL1*	E2	c.383C>T	p. Ala128Val
N52	chr1	exonic	missense variant	*TAL1*	E2	c.184G>C	p. Gly62Arg
N38	chr19	exonic	missense variant	*TCF3*	E18	c.1592C>T	p. Thr531Met
N51	chr4	exonic	missense variant	*TET2*	E11	c.4874C>T	p. Ala1625Val
N51	chr4	exonic	missense variant	*TET2*	E3	c.2667T>G	p. Phe889Leu
N51	chr4	exonic	missense variant	*WHSC1*	E10	c.1910C>T	p. Ser637Leu
N31	chr7	exonic	missense variant	*XRCC2*	E2	c.85C>T	p. Pro29Ser

doi:10.6342/NTU202301505